第33卷 第8期 焊 接 学 报 Vol. 33 No. 8
2012年8月 TRANSACTIONS OF THE CHINA WELDING INSTITUTION August 2012

7A52铝合金电子束焊接参数及性能

翟熙伟[1]， 陈芙蓉[1]， 毕良艳[1]， 张传臣[2]
(1. 内蒙古工业大学 材料科学与工程学院，呼和浩特 010051；
2. 北京科技大学 材料科学与工程学院，北京 100083)


翟熙伟

摘 要： 对20 mm厚7A52铝合金板材采用试件法进行电子束焊接，确定了焊接参数并对力学性能进行分析. 结果表明，采用加速电压60 kV，电子束流120 mA，聚焦电流763 mA，焊接速度800 mm/min，可得到良好的焊缝表面. 电子束流增大焊缝深宽比显著增加，聚焦电流微小的数值变化可引起焊缝形状突变. 接头焊缝区晶粒细小均匀，抗拉强度为母材的87%，焊缝维氏硬度最低值为母材的61%，焊缝冲击韧度为母材的95.4%，表明了电子束接头的性能很高.

关键词： 7A52铝合金；电子束焊接；焊接参数；力学性能
中图分类号： TG4563 **文献标识码：** A **文章编号：** 0253－360X(2012)08－0073－04

0 序 言

7A52铝合金属于Al-Zn-Mg-Cu系超硬铝合金，该合金具有高的比强度、硬度、热加工性能好、塑性好、焊接性能优良、耐蚀性和韧性好等优点，是建筑、航空航天器、地面车辆和装备的主要焊接结构材料[1]. 但该合金在焊接时存在焊缝强度低、焊接接头耐磨性差和疲劳强度低等问题. 特别是对于中厚板(20～60 mm)的焊接，该类问题更加突出. 因此焊接7A52铝合金要求采用能量密度集中、热输入小、焊接速度高的高效焊接方法[2,3].

电子束焊可以在真空环境下利用会聚的高速电子流轰击工件接缝处产生热能，使被焊金属熔合. 电子束作为焊接热源的突出特点是功率密度高、穿透能力强、精确、快速、可控、保护效果好[4-6]. 文中针对厚板7A52铝合金，用试件法确定了电子束焊接参数，通过调整焊接参数控制焊缝形状和焊接接头力学性能，为超硬铝合金电子束焊接的基础研究和工程应用做出了探索.

1 试验方法

焊接母材为20 mm厚的7A52铝合金轧制板材，其化学成分见表1. 试验方法采用试件法，选用ЭЛУ-k1中压电子束焊机，最大加速电压为60 kV. 试验分两步骤完成，首先通过对焊接设备的调控，在焊接过程中实现焊接参数连续变化，焊接工艺参数见表2，并在试件不同参数区域进行线切割取样，经打磨、抛光和腐蚀后对焊缝形状进行对比，得到最优工艺参数；之后采用所得最优工艺参数实施焊接，对试件焊缝形状和力学性能进行检测.

表1 7A52铝合金的化学成分(质量分数，%)
Table 1 Chemical compositions of 7A52 alloy

Zn	Mg	Cu	Mn	Cr
4.0～4.8	2.0～2.8	0.05～0.20	0.20～0.50	0.15～0.25
Ti	**Zr**	**Fe**	**Si**	**Al**
0.05～0.18	0.05～0.15	≤0.30	≤0.25	余量

表2 电子束焊接工艺参数
Table 2 Welding parameters of EBW

试件编号	聚焦电流 I_f/mA	电子束流 I_b/mA	焊接速度 v/(mm·min^{-1})
1	760	80～110	800
2	760	110～120	800
3	754～760	120	800
4	760～764	120	800

2 试验结果与分析

2.1 电子束流变化下的焊缝形貌

电子束焊接的主要工艺参数包括加速电压U_a、

收稿日期：2011－11－04
基金项目：内蒙古自治区自然科学基金资助项目(2010MS0805)

电子束流 I_b、聚焦电流 I_f、焊接速度 v 和工作距离. 由于在大多数电子束焊接中,加速电压往往不变,为满足不同焊接工艺的需要,常常要调节电子束流值. 文中试验加速电压为 60 kV,1 号和 2 号试件聚焦电流为 760 mA,焊接速度为 800 mm/min,频率为1 100 Hz 的圆形扫描. 1 号试件电子束流从 80 mA 连续变化到 110 mA,2 号试件电子束流从 110 mA 连续变化到 120 mA. 焊后在 1 号和 2 号试件上,依据电子束流增量的步长计算出不同电子束流值所对应的焊缝截面位置,截取 8 个焊缝截面,形貌如图 1 所示,8 个截面对应的形状参数见表 3.

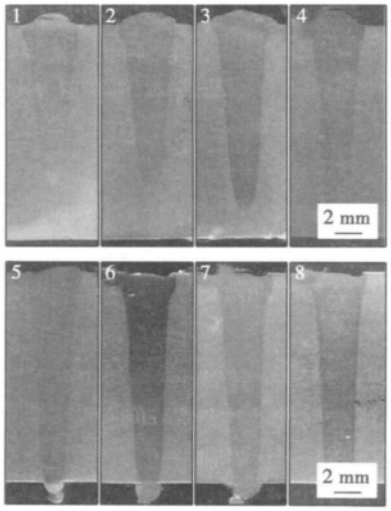

图 1 不同电子束流的焊缝截面形貌

Fig. 1 Weld across-section shape under different beam current

表 3 不同电子束流的焊缝形状参数

Table 3 Weld shape parameters under different beam current

截面编号	电子束流 I_b/mA	实际熔深 H/mm	熔宽 B/mm	焊缝宽度 W/mm	深宽比 H/B	是否焊透	正面质量	背面质量
1	85	14.72	2.70	4.20	5.45	否	差	—
2	90	16.12	3.62	4.44	4.45	否	差	—
3	100	17.12	3.48	4.92	4.92	否	差	—
4	105	18.74	3.36	4.22	5.58	否	差	—
5	107	21.60	3.61	4.68	5.98	是	中	差
6	110	21.82	3.08	4.22	7.08	是	中	中
7	115	22.14	3.16	4.14	7.01	是	良	良
8	120	24.20	3.14	4.10	7.71	是	优	良

结合图 1 和表 3 可知,1 号试件以 I_b = 80 mA 起焊,未焊透,随着电子束电流的增加,当 I_b = 106 mA 时焊透,继续增加至 I_b = 110 mA 时结束. 焊接过程中,未焊透时试件正面呈现周期性变化,焊缝余高和宽度都相应变化;开始焊透时背面连续,焊缝宽度为 2.0 mm,余高为 1.5 mm;焊透后焊缝变得连续、均匀,焊缝接近结束时,连续性较好,余高起伏均匀,焊缝背面宽度大约为 2.2 ~ 2.3 mm,焊缝中心交于基体. 2 号试件以 I_b = 110 mA 起焊时已焊透,增加电子束电流至 120 mA 时结束. 正面都较均匀,焊缝中心交于基体. 随着焊接电流的增加,宽度增加,余高的变化较小,在 I_b = 120 mA 时背面焊缝均匀、连续性好,余高的起伏变化小,中途无突变.

电子束流与焊缝形状参数的关系曲线见图 2. 文中试验所测熔深为实际深度,其中含焊透后钉状焊缝在试件外的余量. 随着电子束流的增大,熔宽和焊缝宽度都呈规律性变化,在焊透前熔宽和焊缝宽度都呈增加趋势,在焊透后熔宽和焊缝宽度都呈下降趋势,但数值变化不大. 而焊缝的实际熔深随着电子束流增大呈明显上升趋势,熔宽略有变化,深宽比增加. 从焊缝外观来看,在保证焊透的前提下,随着电子束流的增大,焊缝正面和背面的质量均明显改善.

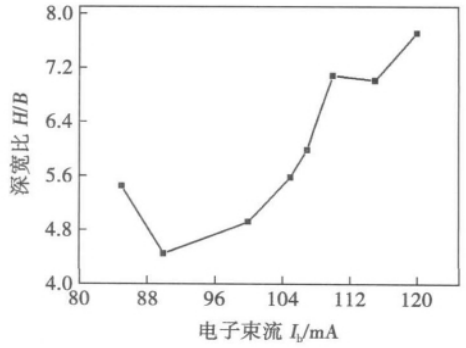

图 2 电子束流对焊缝形状参数的影响

Fig. 2 Effect of weld shape parameters on beam current

2.2 聚焦电流变化下的焊缝形貌

聚焦电流是电子束焊接的重要参数,聚焦电流的取值和焦点的位置对焊缝形状影响很大. 在实际工程应用中,当焊件厚度大于 10 mm 时,一般采用下焦点焊,文中试验即采用下焦点焊,焦点位于熔深的 30% 处,文中试验着重对聚焦电流取值范围进行测试. 焊接工艺参数见表 2,3 号和 4 号试件电子束流 I_b = 120 mA,焊接速度 v = 800 mm/min,3 号试件聚焦电流值由 754 mA 连续变化到 760 mA,4 号试件聚焦电流值由 760 mA 连续变化到 764 mA. 依据聚焦电流增量的步长计算出不同聚焦电流值所对应的焊缝截面位置,截取 5 个焊缝截面,焊缝形貌如图 3 所示,5 个截面对应的形状参数见表 4.

结合图 3 和表 4 可知,3 号试件以 I_f = 754 mA

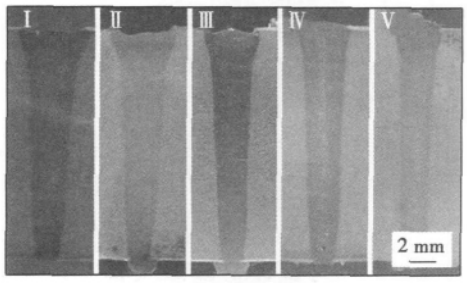

图 3　不同聚焦电流的焊缝截面形貌

Fig. 3　Weld section shape under different focus current

表 4　不同聚焦电流的焊缝形状参数

Table 4　Weld shape parameters under different focus current

截面编号	聚焦电流 I_f/mA	实际熔深 H/mm	熔宽 B/mm	焊缝宽度 W/mm	深宽比 H/B	正面质量	背面质量
Ⅰ	754	22.24	3.52	4.32	6.32	中	差
Ⅱ	757	22.21	3.68	4.52	6.04	中	差
Ⅲ	760	22.18	3.18	4.12	6.97	良	良
Ⅳ	763	22.36	3.08	4.08	7.26	优	良
Ⅴ	764	22.38	3.14	3.58	7.12	差	差

起焊,已焊透,正面焊缝连续、较均匀,但咬边严重,焊缝低于基体深度 0.7 mm,背面焊缝连续但余高波动较大. 随着聚焦电流的增加,咬边量减小,当 I_f = 760 mA 时,焊缝略高于基面,且连续、均匀. 4 号试件以 I_f = 760 mA 起焊,I_f = 760 ~ 763 mA,正面焊缝较均匀,焊缝中心交于基体,无突变. $I_f \geqslant 764$ mA 时,焊缝呈现周期性的脉动,正面和背面的余高和宽度也呈周期性变化,焊缝产生类似放电性的小坑. 电子束流与深宽比的关系曲线见图 4,随着聚焦电流的变化,深宽比变化显著,聚焦电流增加,深宽比先增大后减小. 可见聚焦电流对焊缝形状的影响作用很大,聚焦电流数值的可调范围较小,微小的数值变化可使焊缝形状产生突变.

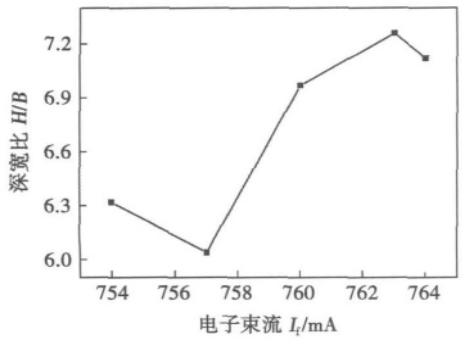

图 4　聚焦电流对焊缝形状参数的影响

Fig. 4　Effect of weld shape parameters on focus current

2.3　其它参数对焊缝形状的影响

文中试验材料曾采用 ZD150-15A 高压电子束焊机,加速电压在 90 ~ 150 kV 范围内试验,虽然对电子束流和聚焦电流数值进行多组调试,但始终是试件被击穿,无法完成焊接. 后改用中压电子束焊机,加速电压 U_a = 60 kV,效果良好. 试验表明,中等厚度的高强铝合金板材适于采用中压电子束焊机.

文中的试验材料属于中等厚度板材,采用焊接速度 v = 800 mm/min,试验所得焊缝形状结果表明,此焊接速度适中,经过对焊缝的 X 射线探伤表明,气孔等缺陷极少.

2.4　焊缝参数优化后的组织性能和力学性能分析

根据图 1、图 3 和表 3、表 4 所示试验结果,选择最优数据,组成优化的参数组如表 5 所示,对材料实施焊接并对组织性能和力学性能进行分析.

表 5　电子束焊接优化参数

Table 5　Welding parameters optimization of EBW

加速电压 U_a/kV	聚焦电流 I_f/mA	电子束流 I_b/mA	焊接速度 v/(mm·min^{-1})
60	763	120	800

2.4.1　焊缝显微组织形貌

图 5 为焊缝显微组织形貌,图 5a 为焊缝边缘显微组织形貌,分为HAZ(A)、熔合线(B)、细晶区

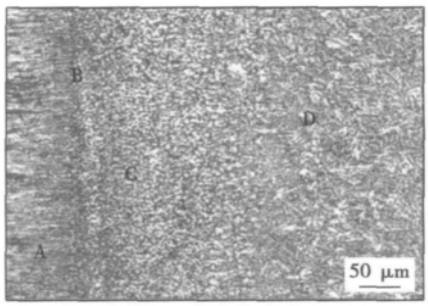

(a) 电子束焊缝边缘显微组织形貌

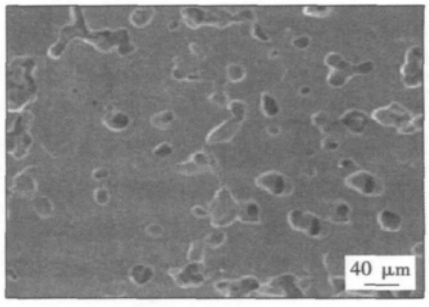

(b) 羽毛状晶区显微组织形貌(SEM)

图 5　焊缝显微组织形貌

Fig. 5　Microstructure of weld

(C)和羽毛状晶区(D),图 5a 中显示出焊缝组织晶粒尺寸比母材细小,熔合线和细晶区的晶粒大小不均匀. 从图 5b 羽毛状晶区形貌可看出,电子束焊缝显微组织的晶粒约为 4 ~ 20 μm,晶粒细小均匀.

2.4.2 焊接接头力学性能

表 6 为 7A52 铝合金电子束焊焊接接头及母材拉伸试验数据,可以看出,电子束焊接头抗拉强度可达母材的 87%,电子束焊接头的断后伸长率小于母材.

表 6 焊接接头与母材拉伸试验数据

Table 6 Tensile test data of joints and base metal

	抗拉强度 R_m/MPa	断面收缩率 Z(%)	断后伸长率 A(%)
母材	523.5	28.7	14.1
试件	455.5	25.8	5.9

在焊缝顶部、中部、底部,分别以焊缝中心为原点,以 1 mm 为步长向左右两侧各取 14 个点测试维氏硬度值,结果显示焊缝中心位置中部的硬度高于焊缝顶部和底部,这是由于在焊接过程中焊缝顶部和底部合金元素 Mg,Zn 蒸发较焊缝中部容易,导致焊缝顶部和底部元素烧损情况较焊缝中部严重,相应的硬度也有所下降. 母材维氏硬度为 170 HV,焊缝顶部维氏硬度最小值为 104 HV,为母材的 61%.

从图 5 可看出,HAZ(A)、熔合线(B)、细晶区(C)交界处,晶粒尺寸突变较大,在受力时易造成应力集中,从而导致电子束焊热影响区冲击韧性下降. 焊接接头冲击试验结果得出,母材冲击韧度为 26.3 J/cm^2,焊缝的冲击韧度为 25.1 J/cm^2,为母材冲击韧度的 95.4%,接头热影响区的冲击韧度为 15.9 J/cm^2,为母材冲击韧度的 60.4%.

3 结 论

(1) 对于中等厚度的 7A52 铝合金板材,采用中压真空电子束焊机,通过调节电子束流、聚焦电流,可以实现良好的焊接,能够满足产品的需求. 对于板厚 20 mm 的 7A52 铝合金板材,采用加速电压 60 kV,电子束流 120 mA,聚焦电流 763 mA,焊接速度 800 mm/min,可得到良好的焊缝表面.

(2) 电子束流对焊缝形状的影响较大,电子束流数值的可调范围较大,随着电子束流的增大,熔宽、熔深、焊缝宽度都呈规律性变化,且深宽比显著增加. 聚焦电流对焊缝形状的影响很大,聚焦电流数值的可调范围较小,微小的数值变化可使焊缝形状突变.

(3) 7A52 铝合金板材电子束焊接接头焊缝区晶粒细小均匀;接头性能优良,接头抗拉强度是母材的 87%;硬度变化区域窄,焊缝维氏硬度最低值为母材的 61%;焊缝的冲击韧度为母材的 95.4%,接头热影响区的冲击韧度为母材的 60.4%.

参考文献:

[1] 潘复生,张丁非. 铝合金及应用[M]. 北京: 化学工业出版社,2006.

[2] 解瑞军,陈芙蓉,张传臣,等. 7A52 铝合金双丝焊工艺及焊缝耐腐蚀性[J]. 焊接学报,2008,29(12): 57 -60.
Xie Ruijun, Chen Furong, Zhang Chuanchen, *et al*. Twin-wire welding technology and corrosion resistance of weld seam for 7A52 aluminum alloy [J]. Transactions of the China Welding Institution, 2008, 29(12): 57 -60.

[3] 逯 瑶,陈芙蓉,解瑞军. 7A52 铝合金焊接接头表面纳米化前后的性能分析[J]. 焊接学报,2011,32(1): 57 -60.
Lu Yao, Chen Furong, Xie Ruijun. Properties of 7A52 aluminum alloy welded joint before and after surface nanocrystallization [J]. Transactions of the China Welding Institution, 2011, 32(1): 57 -60.

[4] 李亚江,王 娟, Puchkov P U. 高能束流焊接技术现状及发展[J]. 航空制造技术,2011(8): 38 -41.
Li Yajiang, Wang Juan, Puchkov P U. Application and development of advanced welding technology by high-energy density beam [J]. Aeronautical Manufacturing Technology, 2011(8): 38 -41.

[5] Wanjara P, Brochu M. Characterization of electron beam welded AA2024 [J]. Contents Lists Available at Science Direct Vacuum, 2010, 85: 268 -282.

[6] 陈国庆,张秉刚,武振周,等. TiAl/Ti60 电子束焊接接头组织及性能[J]. 焊接学报,2009,30(12): 41 -45.
Chen Guoqing, Zhang Binggang, Wu Zhenzhou, *et al*. Microstructure and mechanical properties of electron beam welded dissimilar TiAl/Ti60 joint [J]. Transactions of the China Welding Institution, 2009, 30(12): 41 -45.

作者简介: 翟熙伟,男,1970 年出生,博士研究生,副教授. 主要从事铝合金电子束焊接方面的研究. 发表论文 9 篇. Email: xiweizhai@163.com

通讯作者: 陈芙蓉,女,教授. Email: cfr7075@163.com

Cu_2Ti in grain boundary of Ti_2Cu. While above 950 ℃, the Al-Cu_2Ti gradually disappeared, and TiB whiskers were mainly distributed on Ti_2Cu. When the holding time was 10 min and brazing temperature was 950 ℃, the maximal joint shear strength was 96 MPa. While the holding time was 20 min and brazing temperature was 930 ℃, and the maximal joint shear strength was 83 MPa.

Key words: Al_2O_3 ceramics; TC4 alloy; brazing parameters; microstructure; shear strength

Microstructure analysis of hardfacing layer by electrode cored with high chromium casting iron XU Jinfeng[1], TANG Zhen[1,2], REN Yongming[1], ZHAI Qiuya[1] (1. School of Materials Science and Engineering, Xi'an University of Technology, Xi'an 710048, China; 2. Xi'an Far East Import & Export Co., Ltd., Xi'an 710077, China). pp 57 - 59, 64

Abstract: The hardfacing electrodes cored with high chromium casting iron were developed to adequately transfer alloying elements. The transfer coefficient was calculated and the microstructure and hardness of the hardfacing layer from different coatings were investigated. The results indicated that the transfer efficiency of electrodes was more than 85%. Different compositions and microstructure in the hardfacing layer can be obtained using the same-cored wire covered with different coatings. When the cored welding-wire was covered with alkalescent low-hydrogen coating, the hardfacing layer with hypoeutectic high chromium casting iron formed and the microstructure consisted of primary austenite γ, martensite M and carbide. While covered with alkalescent graphite coating, the hardfacing layer with hypereutectic high chromium casting iron was formed and the microstructure consisted of primary carbide, martensite M, carbide Fe_7C_3 and a small amount of G. Since hard Cr_7C_3 and martensite phases existed in the hardfacing layer, the hardness of the hardfacing layer was high. The hardness of the hypoeutectic and hypereutectic high chromium casting iron hardfacing layers was 44.5 - 56.5 HRC and 59-67 HRC, respectively.

Key words: high chromium casting iron; hardfacing electrode; transfer coefficient; microstructure of hardfacing layer

Weld hot crack analysis of 6005A aluminum alloy profile for high-speed train ZHANG Jian, LEI Zhen, WANG Xuyou (Harbin Welding Institute, Mechanical Science Research Institute, Harbin 150080, China). pp 60 - 64

Abstract: The hot cracking sensibility of 6005A aluminum alloy was investigated with hot plasticity test, and the weld hot crack of 6005A aluminum alloy profile in laser-MIG hybrid welding was analyzed. Hot plasticity test results indicated that the brittle temperature range (BTR) of 6005A aluminum alloy was 550-640 ℃, which demonstrated that the hot cracking sensibility of the aluminum alloy was high. High-efficient welding of 6005A aluminum alloy profile can be achieved by utilizing laser-MIG hybrid welding process with I groove and welding speed up to 4.5 m/min. However, hot crack perpendicular to weld bead was found on the back of weld. The increase of dilution rate, caused by changing the groove, was the main reason for the generation of hot crack on the back of weld made by laser-MIG hybrid welding. However, the hot crack can be avoided by using V groove instead of the I groove in the hybrid welding of 6005A aluminum alloy profile.

Key words: aluminum alloy profile; brittle temperature range; hot crack; laser; hybrid heat resources

Effects of interpass temperature on crack propagation energy in deposited metal of 690 MPa grade HSLA steel WANG Aihua, PENG Yun, XIAO Hongjun, TIAN Zhilin (State Key Laboratory of Advanced Steel Processes and Products, Central Iron & Steel Research Institute, Beijing 100081, China). pp 65 - 68, 72

Abstract: Instrumented impact test was conducted on the deposited metal of 690 MPa grade HSLA steel when the interpass temperature was 80 ℃ and 200 ℃, respectively. The factors to hinder crack propagation were discussed with optical microscope (OM), scanning electron microscope (SEM) and electron backscatter diffraction (EBSD) combining with load-distance curve. The results showed that the impact energy of the deposited metals made with interpass temperature of 80 ℃ and 200 ℃ was 103.9 J and 63.2 J, respectively. The gap between crack initiation energy and propagation energy was 6.7 J and 34 J for two interpass temperatures, respectively. The difference of impact energies was mainly attributed to the propagation energy. During the crack propagation, the maximum propagation distance of the dimple area was 1.68 mm and 0.6 mm for 80 ℃ and 200 ℃ of interpass temperature, respectively. The fractography of the brittle fracture areas was mainly of cleavage, but dimple bands were observed in the deposited metal with interpass temperature of 80 ℃. It was concluded that the proportion of high angle grain boundaries of 55° - 60° determining the impact energy.

Key words: interpass temperature; impact toughness; crack propagation; high angle grain boundary

Microstructure and mechanical properties of YAG pulse laser butt joint of thin AZ61 magnesium alloy sheets LI Zhijun, WANG Hongying (The Industrial Training Center, Shenzhen Polytechnic, Shenzhen 518055, China). pp 69 - 72

Abstract: YAG pulse laser welding of thin AZ61 magnesium alloy sheets was conducted. The microstructure and chemical compositions of the welded joint were examined with optical microscope (OM) and energy dispersive X-ray analysis (EDX), and the microhardness and tensile strength of the joints were measured. The results show that the weld front side slightly collapsed but the weld back side shaped well. The weld had good appearance and solid mechanical properties. The grain was finer and the microhardness was higher in the fusion zone than that in the base metal. The tensile strength of the joint was 250 MPa, equivalent to that of the base metal. The evaporation of Mg led to the increasing of Al content in the weld, but the Zn content was low.

Key words: AZ61 magnesium alloy; laser welding; microstructure; mechanical property

Welding parameters and mechanical properties of electron beam welding of 7A52 aluminum alloy ZHAI Xiwei[1], CHEN Furong[1], BI Liangyan[1], ZHANG Chuanchen[2] (1. College of Material Science and Engineering, Inner Mongolia University of Technology, Hohhot 010051, China; 2. School of Materials Science and Engineering, University of Science and Technology Beijing, Beijing 100083, China). pp 73 - 76

Abstract: The electron beam welding of 20 mm 7A52 aluminum alloy plates was conducted. The welding parameters were determined by the method of multiple specimens and the mechanical properties of the joints were examined. The results showed that the satisfing weld appearance can be achieved when the accelerating voltage was 60 kV, electron beam current was

120 mA, focus current was 763 mA and welding speed was 800 mm/min. The ratio of depth to width obviously increased with the increase of electron beam current. Tiny alteration of focus current caused significant change in the weld shape. Fine and uniform grains occurred in the weld seam, and the fracture strength, weld hardness and impact toughness of the joint reached 87%, 61% and 95.4% of those of base metal, respectively.

Key words: 7A52 aluminum alloy; electron beam welding; welding parameters; mechanical properties

Performance of dissimilar metal weld between SA335P91 and 12Cr1MoV steels in ultra(ultra) supercritical thermal power units ZHENG Kai[1,2], ZHAO Dajun[1], ZHANG Xuelian[3] (1. College of Construction Engineering, Jilin University, Changchun 130022, China; 2. Vocational and Technical College, Jilin Architectural and Civil Engineering Institute, Changchun 130118, China; 3. Guangdong Yudean Group Co., Ltd., Guangzhou 510630, China). pp 77 – 80

Abstract: Dissimilar metal welds between SA335P91 and 12Cr1MoV ferritic heat-resistant steels are widely applied in the main steam pipe and the reheater on boiler heating surface for the supercritical (SC) and ultra-supercritical (USC) thermal power units in China. The characteristics of microstructure and weldability of two steels were described, and the welding mechanism for dissimilar metal weld between two steels was investigated. Through theoretical analysis and experiments, the main factors in dissimilar metal welding that resulted in hot and cold cracks, decrease of toughness, embrittlement and type IV softening cracking tendency were determined. Corresponding technological methods and heat treatment procedures to prevent the above defects were proposed and solid joints were achieved.

Key words: supercritical; ultra-supercritical; dissimilar heat resistant steel; ferrite; welding

Microstructure and mechanical properties of thick titanium alloy joint in narrow-gap TIG welding LÜ Shixiong[1], CUI Qinglong[1], HUANG Yongxian[1], ZHENG Chuanqi[1], WANG Yang[2] (1. State Key Laboratory of Advanced Welding and Joining, Harbin Institute of Technology, Harbin 150001, China; 2. Qianjiang Motorcycle Co., Ltd., Wenling 317500, China). pp 81 – 84

Abstract: High-quality joint of thick TC4 titanium alloy plate was made by narrow-gap tungsten inert gas (TIG) welding with proper gas protection and welding parameters. Metallographic analysis of the resultant joints revealed the rules of grain growth and microstructure characteristics. The variation of the cooling speed resulted in different microstructures in the heat-affected zone (HAZ). The tensile test showed that the average tensile strength of the joints reached 90% of that of the base metal, which was attributed to the mechanism of meshing strengthening during narrow-gap TIG welding of thick titanium alloy plate.

Key words: thick titanium alloy plate; narrow-gap TIG welding; microstructure; mechanical property

Effects of surface absorption of Ge on Sn2.5Ag0.7Cu/Cu interfacial reaction and wettability YANG Tuoyu[1], MENG Gongge[2], CHEN Feng[1], XIA Xianming[1] (1. School of Mechanical Electronic and Vehicle Engineering, Anhui Science and Technology University, Anhui 233100, China; 2. School of Materials Science and Engineering, Harbin University of Science and Technology, Harbin 150040, China). pp 85 – 88

Abstract: The evolution of wetting property and interfacial morphology of Sn2.5Ag0.7Cu solder was investigated before and after adding active elements. The spreading areas of solder with different contents of Ge were measured, and the morphology of the compound was analyzed with SEM. The relationship between tension on the solid-liquid interface and the absorption amount of active elements on the same place during soldering and its effect on wetting properties were studied. The results showed that when the Ge content in solder was 0.5%, its absorption on the interface quickly raised, the forward-growing tendency of the compound was strong, and the spreading area was the largest. When the Ge content in solder was 1.0%, the absorption remained obvious but the wetting performance was weakened, and the thickness of the compound was relatively thinner. This phenomenon indicates that Ge can reduce the tension on the soldering interface within a certain range. In addition, when the absorption was relatively large, the diffusion between Cu and solder can be restrained and the growth of the compound can be hindered.

Key words: lead-free solder; active element; soldering interface; adsorption

Influence factors of dynamic recrystallization of 7050 aluminium alloy friction stir weld ZHANG Chengcong[1], CHANG Baohua[1], TAO Jun[2], ZHANG Tiancang[2] (1. Key Laboratory for Advanced Materials Processing Technology, Ministry of Education, Tsinghua University, Beijing 100084, China; 2. Research Office for Aero Engine Technology, Beijing Aeronautical Manufacturing Technology Research Institute, Beijing 100024, China). pp 89 – 92

Abstract: Friction stir welding of 7050 aluminum alloy under different rotation rates and tool traverse speeds was conducted and the influence of welding parameters on the grain size of nugget zone was investigated. To analyze the affecting mechanism of welding parameters on the grain size of nugget zone, isothermal compression experiments under different strain rates and deformation temperatures were performed and the influence of deformation parameters on the dynamic recrystallization was analyzed. Results showed that grain size in nugget zone changed slightly with the increase of the rotation rate, while it decreased with the increase of tool traverse speed. Within the range of complete dynamic recrystallization, the recrystallization grain size decreased with increase of the value of ln$Z$. The welding parameters affected the Zenner-Hollomon parameter and then determined the grain size in nugget zone.

Key words: 7050 aluminum alloy; friction stir welding; dynamic recrystallization; thermal-physical simulation

Analysis on mechanism of removing oxide film on stainless steel by heating in low vacuum HE Peng[1], ZHENG Yansong[1], LI Jun[1,2], QIAN Yiyu[1], LOU Haoyue[2], ZHANG Wenfeng[2] (1. State Key Laboratory of Advanced Welding and Joining, Harbin Institute of Technology, Harbin 150001, China; 2. Yinlun Machinery Co., Ltd., Taizhou 317200, China). pp 93 – 96

Abstract: In low vacuum condition, 0Cr18Ni9 stainless steel sheets, with one in supply state and the other pre-oxidized at 800 ℃ in air, were heated, and the steel sheet in supply state